Buckling and post-buckling behavior of auxetic cellular structures

M. Belhadjamor, S. Belghith, M. Ben Bettaieb, S. Mezlini, F. Abed-Meraim

▶ **To cite this version:**

M. Belhadjamor, S. Belghith, M. Ben Bettaieb, S. Mezlini, F. Abed-Meraim. Buckling and post-buckling behavior of auxetic cellular structures. Proceedings of the Institution of Mechanical Engineers, Part L: Journal of Materials: Design and Applications, 2025, 239 (4), pp.680-693. ⟨10.1177/14644207241305697⟩. ⟨hal-04884732⟩

HAL Id: hal-04884732

https://hal.science/hal-04884732v1

Submitted on 13 Jan 2025

HAL is a multi-disciplinary open access archive for the deposit and dissemination of scientific research documents, whether they are published or not. The documents may come from teaching and research institutions in France or abroad, or from public or private research centers.

L'archive ouverte pluridisciplinaire **HAL**, est destinée au dépôt et à la diffusion de documents scientifiques de niveau recherche, publiés ou non, émanant des établissements d'enseignement et de recherche français ou étrangers, des laboratoires publics ou privés.

HAL Authorization

Buckling and post-buckling behavior of auxetic cellular structures

M BelHadjAmor[1,2], S Belghith[2], M Ben Bettaieb[3,4], S Mezlini[2] and F Abed-Meraim[3,4]

Abstract

In this work, experimental tests and numerical simulations are carried out to investigate the buckling behavior and failure modes of auxetic cellular structures and sandwich panels with auxetic cores. Different Poisson's ratios and densities are considered to evaluate the impact of these parameters on the deformation mechanisms under uniaxial compression loading. The numerical analysis is performed using the Riks method, while considering geometric nonlinearity and elastoplastic behavior. The results indicate that negative Poisson's ratio and structure density have a significant influence on the buckling critical stress and the failure mechanisms of cellular structures. Although the inverted honeycomb and the double arrowhead with different Poisson's ratios exhibit similar load capacity, facesheet failure is more pronounced with the conventional inverted honeycomb. This result can be attributed to the dominant effect of the facesheet on the load evolution. The effects of the cell-wall thickness and the facesheet thickness on the buckling load are also discussed based on the finite element model.

Introduction

Honeycomb sandwich structures are well known for their outstanding features, including low weight, high strength, and enhanced energy absorption, making them ideal for a wide range of applications in various fields. Conventional honeycomb structures exhibit a positive Poisson ratio. By inverting this configuration, structures with a negative Poisson ratio, known as auxetics, have been developed to achieve superior mechanical properties in sandwich panels.[1] The term auxetic, first suggested by Evans et al.,[2] describes a material or structure that contracts in the transverse direction under uniaxial compressive loads. Besides the inverted honeycomb structure, which is the traditional and most famous auxetic form, other auxetic forms have been designed and evaluated.[3] Auxetic structures have demonstrated numerous engineering benefits, including high indentation resilience,[4] high shear resistance,[5] and improved energy absorption.[6] Particularly, the compressive mechanical properties of auxetic structures have been thoroughly investigated. Dong et al.[7] studied the compressive behavior of auxetic inverted honeycombs by evaluating the effects of cell-wall thickness and cell number. Experiments and numerical simulations have been conducted to study the deformation modes, energy absorption, and crushing stress as functions of the negative Poisson ratio. Novel auxetic unit cells have been designed by making modifications to the conventional auxetic forms, such as adding wedge-shaped parts,[8] embedding a rhombic configuration,[9] and combining positive and negative Poisson's ratios.[6] The numerical topology optimization method has been widely used to design novel and optimal auxetic structures since the pioneering work of Larsen et al.[10] Using this method, Bohara et al.[11] have proposed an optimum topology of auxetic unit cells aimed at maximizing energy absorption. These newly developed auxetic structures

[1]Laboratoire de Génie Mécanique, Ecole Nationale d'Ingénieurs de Monastir, Université de Monastir, Monastir, Tunisie
[2]Ecole Nationale d'Ingénieurs de Carthage, Université de Carthage, Tunis, Tunisie
[3]Université de Lorraine, CNRS, Arts et Métiers Institute of Technology, Metz, France
[4]DAMAS, Laboratory of Excellence on Design of Alloy Metals for low-mAss Structures, Université de Lorraine, Lorraine, France

Corresponding author:
M BelHadjAmor, Laboratoire de Génie Mécanique, Ecole Nationale d'Ingénieurs de Monastir, Université de Monastir, 5019 Monastir, Tunisie; Ecole Nationale d'Ingénieurs de Carthage, Université de Carthage, 2035 Tunis, Tunisie.
Email: meriem.belhadjamor@gmail.com

have shown superior properties compared to conventional auxetic forms.

Due to their advantageous properties, which arise from negative Poisson's ratios, auxetic structures are considered as potential candidates for designing cores of sandwich panels to provide enhanced functional properties and to expand the application range beyond conventional honeycombs. Recently, numerous research studies have been performed to investigate the bending,[12] linear buckling, and vibration responses of sandwich plates with auxetic cores.[1] The variational asymptotic method is also often used to study the buckling response of composite auxetic sandwich panels, which are prone to buckle under compressive loads or bending moments. Using this method, Xiao et al.[13] have investigated the buckling behavior of a sandwich plate with an aluminum auxetic honeycomb core as well as laminated composite facesheets. They evaluated the effects of negative Poisson's ratios of the core on the critical buckling load, assuming linear constitutive model and geometric nonlinearity. Subsequently, Xiao et al.[14] used a particle warm optimization algorithm to optimize the buckling loads and natural frequencies of composite inverted honeycomb sandwich panels. Zhen et al.[15] have investigated the static displacement, global buckling, and free vibrations of triangular honeycomb sandwich panels using the variational asymptotic method. Furthermore, the influences of structural parameters and unit-cell form have been discussed. They found that, compared to three other honeycomb geometries, triangular honeycomb sandwich panels show excellent buckling and bending resistances. Liu et al.[1] proposed a novel type of butterfly-shaped auxetic core sandwich plate and evaluated the effect of its negative Poisson's ratio on the buckling and post-buckling behavior using an equivalent model established by the variational asymptotic method. Although these studies focused on the buckling and post-buckling responses of auxetic core sandwich panels, which can lead to catastrophic failure, they were limited to elastic buckling with linear elastic constitutive models.

The plastic buckling failure of sandwich panels has been widely addressed in the literature for sandwich structures with conventional honeycomb cores,[16] beetle elytron cores,[17] and fluted cores.[18] Vinson[19] developed an analytical model enabling the optimization of honeycomb composite sandwich structures by considering possible buckling modes, namely, overall (global) buckling, core shear instability, face wrinkling, and monocell buckling. He stated that "the sandwich panel is rendered useless if any of the four modes of buckling occurs". Analytical solutions have also been proposed for the analysis and design of minimum weight composite sandwich panels with honeycomb core subjected to in-plane uniaxial compressive loads.[19] To explore the crushing behavior of aluminum honeycomb sandwich panels, Sun et al.[20] conducted a comprehensive study based on three-point bending and in-plane compression tests, as well as finite element models taking into account the adhesive interface between the facesheets and honeycomb core. Critical buckling loads and failure modes were predicted for different facesheets and core-wall thicknesses. It was shown that the structural parameters of the honeycomb core and facesheets significantly impact the maximum load, energy absorption, and specific energy absorption. These crashworthiness criteria exhibit strong dependence on the mechanical behavior, including yield stress and buckling load, of the facesheets. Zhang et al.[17,21,22] have developed analytical, numerical and experimental studies to investigate the buckling behavior of beetle elytron-inspired sandwich panels, which are considered as key components for structural bending resistance. Analytical and numerical models were proposed to predict the local buckling load of the compressive skin that controls the failure of the sandwich panel subjected to bending under lateral loads. Numerical results were validated experimentally by a series of static four-point bending and shear tests aiming at studying the buckling and post-buckling behavior of 3D printed PLA beetle elytron-inspired sandwiches. Based on the experimental results, the bioinspired sandwich panels showed maximum improvement of approximately 35% in post-buckling stress of the compressive skin and enhancement of about 2.8 times in shear buckling stress, as compared to conventional grid sandwich plates. Li et al.[18] have explored, based on analytical models, the failure mechanisms of fluted-core sandwich composite panels under uniaxial compression, including global buckling, local buckling, and material failure. Finite element models and in-plane uniaxial compression tests were performed according to the standard test method ASTM C364. Failure mode maps of fluted-core composite sandwich panels were established to illustrate the relationship between geometric parameters and panel failure modes.

In this article, we aim to study the plastic buckling of auxetic structures and sandwich panels with negative Poisson's ratio core. The buckling behavior of specimens with different auxetic re-entrant structures and different densities is first experimentally investigated. Uniaxial compression tests are carried out to evaluate the ultimate strength of different specimens and their buckling failure modes. Different numerical approaches have been used in the literature to predict the onset of buckling, namely, the bifurcation theory[23] and the limit-point method.[24,25] In the present paper, the Riks path-following technique, which is a limit-point method, is employed to predict the buckling and post-buckling of these auxetic cellular structures and sandwich panels with auxetic cores, while accounting for their plastic behavior. Experimental and numerical results are compared to evaluate the accuracy of the developed approach.

Buckling tests and finite element models

Geometric configurations

As previously indicated, there are many types of auxetic structures in the literature. In this work, two of the most known configurations are chosen: (i) the inverted (or

re-entrant) honeycomb (IHC) obtained by inverting a regular hexagon,[26] and (ii) the double arrowhead (DAH) structure, also called re-entrant quadrilateral, firstly identified by Larsen et al.[10] using a numerical topology optimization method. Figure 1 depicts the chosen structures and the geometric parameters of the considered specimens. For a fair comparison, all specimens have nearly the same dimensions: length (L), width (W), and out-of-plane height (H) of $L = 100$ mm, $W = 50$ mm, and $H = 8.42$ mm, respectively. The height of the core (h_c) and the facesheet thickness (t_f) are also set to $h_c = 6.82$ mm, $t_f = 0.8$ mm, respectively.

The key geometric parameters of the re-entrant honeycomb and the double arrowhead unit cells are illustrated in the same figure. These parameters include the internal angles (θ and φ), the lengths of the cell ribs (l_1 and l_2), and the cell-wall thickness t_c, which is set to 0.5 mm. Table 1 summarizes the design parameters of the considered auxetic unit cells denoted IHC, DAH1 and DHA2.

The design parameters of the unit cell control the in-plane mechanical properties of the auxetic structures, particularly, the relative density and the Poisson ratio. The relative densities of IHC and DAH cells are given by Equation (1)[27] and (2),[28] respectively:

$$\frac{\rho^*}{\rho_m} = \frac{t_c / l_1 (l_2 / l_1 + 2)}{2\cos\theta (l_2 / l_1 + \sin\theta)} \tag{1}$$

$$\frac{\rho^*}{\rho_m} = \frac{t_c \, (\sin\varphi - \sin\theta)}{l \, \sin(\varphi - \theta)} \tag{2}$$

where ρ^* and ρ_m represent the density of the unit cell and the base material density, respectively. The Poisson ratio expressions for the IHC and DAH cells, subjected to loading in the $\boldsymbol{x}$ direction, are given by Equation (3)[27] and (4),[28] respectively.

$$\nu_{xy} = \frac{(t_c / l_1 + \sin\theta)\sin\theta}{(\cos\theta)^2} \tag{3}$$

$$\nu_{xy} = \frac{-1}{\tan\varphi \tan\theta} \tag{4}$$

As the auxetic behavior of these re-entrant geometries is primarily dependent on the internal angles that control the Poisson ratio of the structure, two values of the angle θ are evaluated for the DAH cell. The relative densities and Poisson ratios of IHC, DAH1, and DHA2 unit cells are listed in Table 1. These values have been obtained for PolyLactic Acid (PLA) material with $\rho_m = 1.2\ g/cm^3$.[29]

Manufacturing and experiments

The designed structures are manufactured using the fused deposition method (FDM), which is widely adopted to fabricate cellular structures from thermosoftening materials. In our study, we have used PolyLactic Acid (PLA) material.[6] A Raise 3D Pro2 printer with a 0.4 mm nozzle size has been used, loaded with Raise3D Premium PLA Filament. The structures have been printed with a layer resolution of 0.2 mm, employing a printing pattern of 45° and −45° along the specimen length direction. Each printed structure, including both the core and the sandwich panel components, is designed as a solid by setting the infill density to 100%. The sandwich panels have been manufactured by simultaneously printing the core and the facesheets under the same printing conditions. Grip zones of length L_f (about 20 mm) have been added for the specimen fixture, as shown in Figure 2. The fabricated structures included a raft, which has been removed after printing. The build direction has been chosen to avoid any support material.

In-plane uniaxial compression tests have been carried out on the printed structures according to the standard test method ASTM C364, using an electronic universal testing machine (Figure 3). To evaluate the buckling behavior of auxetic structures, a sandwich panel with an auxetic core as well as a cellular auxetic structure have been manufactured and tested for each cell presented in Table 1. The specimen composed of an auxetic core with two relatively thin facesheets is denoted with the prefix "SP_". The auxetic cellular structure (core without facesheets) is denoted with the prefix "C_". The grip zones of the specimens have been fixed into the test fixtures. A uniaxial compression load has been applied on the top fixture at a loading rate of 0.5 mm/min to ensure quasi-static buckling. For each specimen type, three samples have been tested. The uniaxial load, displacement, and time have been recorded by a 20 kN load sensor integrated into the testing machine, with a load resolution of 1 N. To quantify the structure deformation during the test, a Digital Image Correlation (DIC) technique has been used. A camera has been employed to capture the structural deformation process. DIC images have been captured by an IMPERX ICL-B1620 camera at a resolution of 1608×1600 pixels and a frame rate of 30 frames per second. Image acquisition has been performed using PIXCI® software (EPIX Inc., Buffalo Grove, USA). Prior to experimental testing, the 3D printed specimens have been covered with a stochastic speckle pattern using spray paint to enhance the capture of the structural deformation behavior. The grey levels of the speckle pattern exhibit a Gaussian distribution, characterized by a mean of 183 and a standard deviation of 57. These grey levels are encoded on 8-bit scale, with pixel values spanning from 0 to 255. The size of each speckle pattern ranges from 1 to 25 pixels. The recorded videos throughout the tests allowed the analysis of the structural deformation and the identification of the buckling modes.

Finite element modeling

The buckling and post-buckling behavior of the auxetic structures have been numerically simulated using the commercial finite element (FE) software ABAQUS. ABAQUS/Standard FE solver offers two numerical methods to study the buckling behavior, namely, the '*Buckle'* module and the Riks method. While the

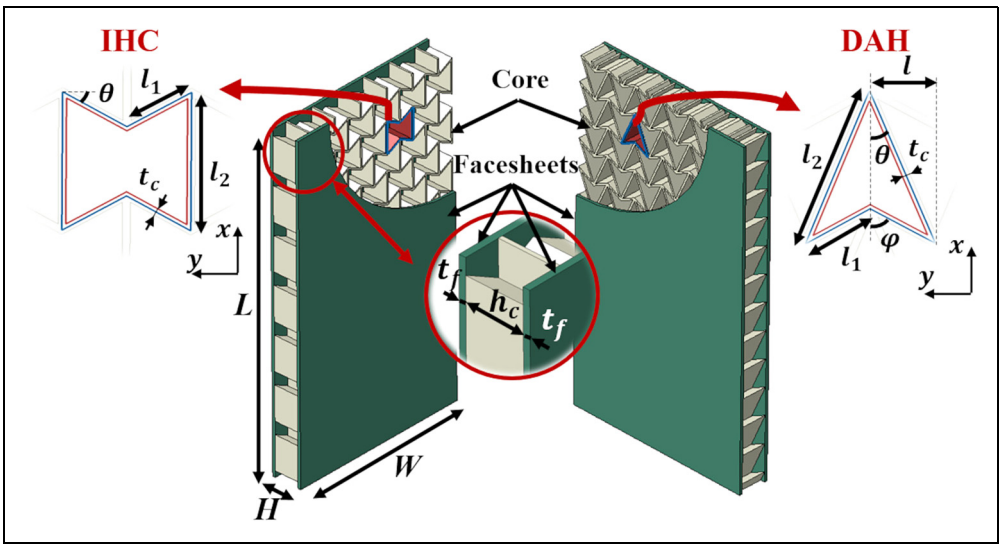

Figure 1. Geometric parameters of the sandwich panel and the unit cells IHC and DAH.

Table 1. Design parameters and properties.

Unit cell	θ	φ	l_1	l_2	l	ν_{xy}	ρ^*/ρ_m
IHC	−30	–	4.8	9.6	-	−1	0.16
DAH1	21.5	60	4.8	11.34	4.15	−1.46	0.19
DAH2	30	60	4.8	8.31	4.15	−1	0.24

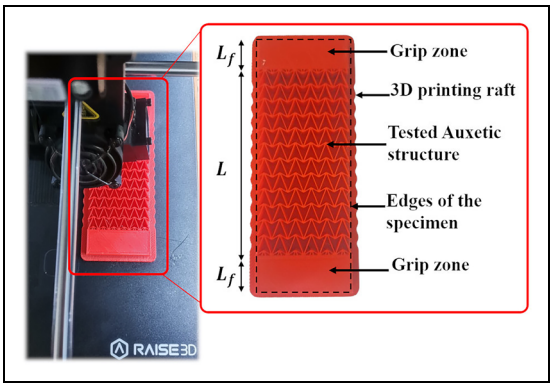

Figure 2. 3D printed specimen.

'*Buckle*' module is limited to predicting elastic buckling load and the associated modes, the Riks method (also known as the arc-length method) allows analyzing elasto-plastic buckling and post-buckling behavior. Given that experimental results indicate elastoplastic behavior, the finite element analysis (FEA) has been carried out using the Riks path-following method to accurately detect both the critical buckling load and the post-buckling behavior. The Riks method is widely used to predict structural instability and to handle geometric nonlinear collapse, relying on the imperfection approach. This approach requires the introduction of initial geometric imperfections to simulate actual imperfections in specimens, which can significantly influence both the critical buckling stress and post-buckling response.[30] These initial imperfections are typically drawn from the buckling modes, generated by the '*Buckle*' module through the linear perturbation analysis. Thus, prior to the application of compressive loading, the structure is slightly deformed along the shape of its dominant eigenmode to replicate the initial conditions that will trigger buckling.

The FEA has been performed by developing two finite element models (FEM):

1. In the first Finite Element Model (***FEM1***), the *Buckle* Module in ABAQUS/Standard has been used to perform a linear eigenvalue buckling analysis, assuming linear material behavior and small displacements (i.e., material and geometric linearity). The elastic buckling stresses and corresponding eigenmodes have been determined.
2. In the second Finite Element Model (***FEM2***), the *Riks* method in ABAQUS/Standard has been employed to perform a nonlinear analysis accounting for geometric and material nonlinearities and considering initial geometric imperfections. These imperfections have been introduced by scaling and adding the first linear buckling eigenmode obtained from ***FEM1***. Our simulations have been conducted with a scaling factor $\emptyset$ set at 10% of the facesheet thickness t_f. The imperfection sensitivity has been investigated to alleviate the effect of imperfections on the numerical results.

A flowchart illustrating the numerical approach and the complementarity roles of these models is presented in Figure 4.

This approach has been applied to simulate the SP_specimens and C_specimens using the finite element models A and B, respectively, as shown in Figure 5. For comparison with experimental results, the geometry, configuration, and boundary conditions of the finite element model are kept the same as in the experimental tests. To

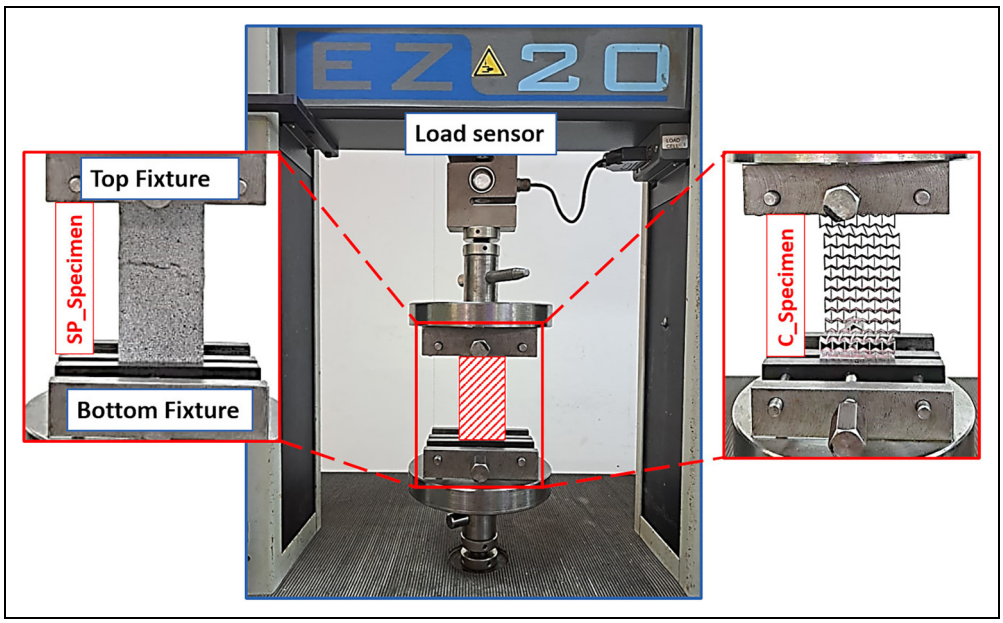

Figure 3. Experimental setup of the uniaxial compression test.

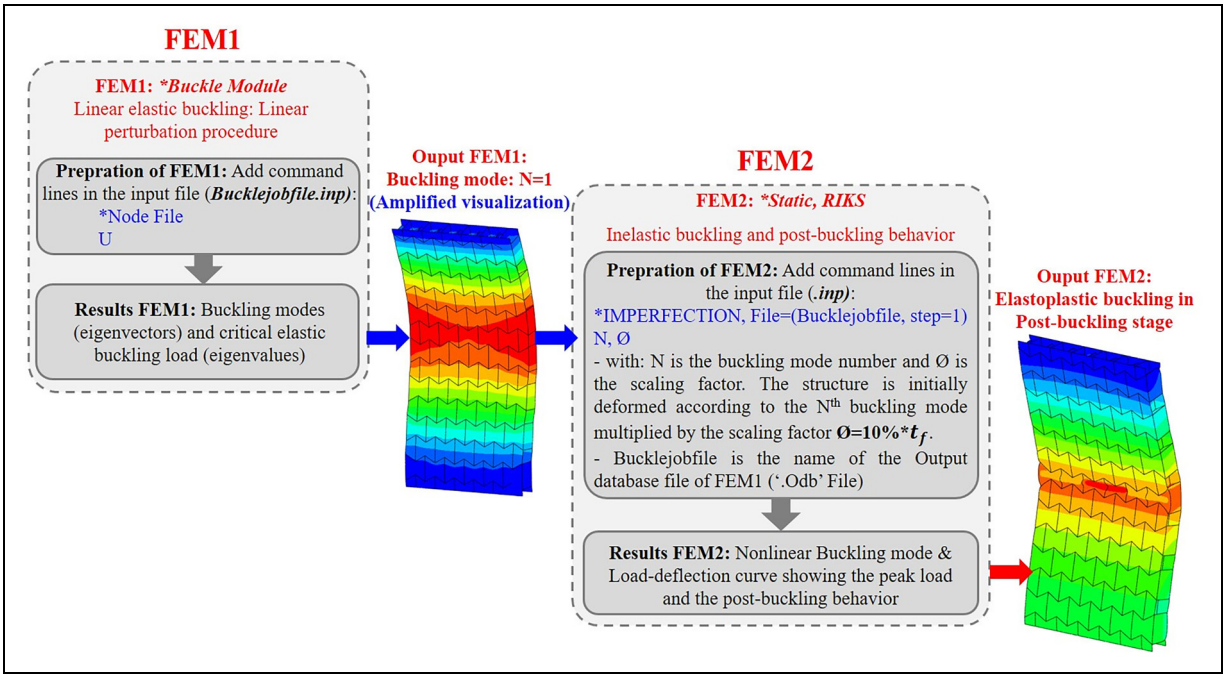

Figure 4. Flowchart of the numerical approach.

achieve simplicity and computational efficiency, grip zones have been eliminated from the simulations. To match the kinematics of the experimental tests, the top and bottom ends of the specimen have been clamped, constraining translation along the z-axis as well as rotations, effectively removing rigid body motions. Uniaxial compression has been applied to the top end to generate buckling loads. The facesheets and the cell walls have been modeled using four-node shell elements (S4) with an element size of 0.8 mm. Each facesheet in the sandwich panels has been discretized into 9916 elements, while the number of elements for the cores has been varied according to the specimen type, as shown in Table 2. The optimal number of elements has been determined based on a mesh sensitivity study. We have selected an elastic perfectly plastic constitutive framework to model the mechanical behavior. According to the Raise3D data-sheet, the Young modulus and the nominal yield strength have been set to 2681 MPa and 40 MPa, respectively.[29] The Poisson ratio of the 3D printed PLA material has been taken as 0.36.[17]

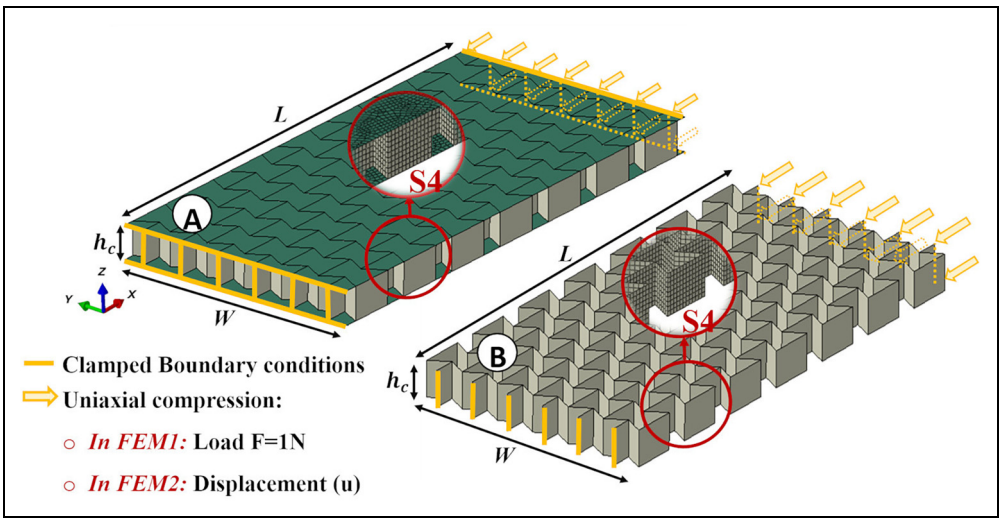

Figure 5. Finite element model: geometry, boundary conditions and mesh: (A) for SP_specimen and (B) for C_specimen.

Experimental results

Buckling of auxetic structures

The load–displacement curves of auxetic structures, namely, IHC, DAH1, and DAH2 and the corresponding deformation process under uniaxial compression are presented in Figure 6(a), (b) and (c), respectively. Three samples of each structure have been tested. The results reveal that the auxetic unit-cell geometry and the structure density significantly affect the critical buckling load, indicated by limit point B on the load–displacement curve, as well as the post-buckling behavior. In the IHC cellular structure (Figure 6(a)), point B marks the onset of transverse symmetric in-plane buckling, leading to loss of axial symmetry. At this point, the structure reaches a critical load of 94.4 N at a displacement of $u = 4.05$ mm, followed by a load reduction. Continued compression of the in-plane global buckling shape leads to the collapse of the first row, which is the least dense cell row consisting of five cells, nearest to the lower fixture. The collapse direction is imposed by the in-plane buckling direction. At this stage, the transverse and axial symmetries are lost. The onset of the densification occurs at $u = 5.52$ mm (point C) when the collapsed cell walls make contact, after which the load rises again, reaching a second limit point (D), corresponding to the second instability stage. Notably, both limit points (B and D) are reached at almost the same critical load and exhibit the same buckling mode. The second point of densification (E) is marked by the collapse of a second row of cells symmetric to the first collapsed row with respect to the transverse plane. Densification points are reached at nearly the same load. These results are in good agreement with those reported in the literature.[27] However, the behavior of the re-entrant honeycomb structure in this study differs from that observed in previous works on pure compression. This difference is mainly due to the higher slenderness ratio (length-to-width ratio) and the clamped edges. These factors promote in-plane buckling rather than compression, leading to the collapse of transversely symmetric rows in an already buckled structure. Figure 6(b) shows that the DAH1 material exhibits roughly the same deformation stages as the IHC structure: shrinking, instability, and densification.[8] However, the gap between the instability and the densification points is reduced, which can be attributed to shorter cell walls. Regarding the response of the DAH2 (Fig. 6(c)), the buckling and post-buckling are characterized by out-of-plane deflection, as shown in the deformed shape at point C. In this case, the structure undergoes elastic buckling, which can be attributed to the high density that makes the structure behavior comparable to that of a continuous plate. By contrast, after unloading, the IHC and DAH1 exhibit in-plane buckling, manifested by buckled and yielded cell walls, as shown in Figure 6. It appears from these results that the DAH2 configuration involves the highest buckling stress, which is somehow mitigated by the increased density. Table 3 provides the specific critical buckling stress of the tested specimens and the involved failure modes. The specific critical buckling stress corresponds to the ratio of the critical nominal stress to the density of the auxetic structure. It is noteworthy that the DAH1 structure, which possesses the most negative Poisson ratio, presents the highest specific critical buckling stress. For the IHC and DAH2 structures, although they have the same Poisson ratio, they exhibit different specific critical buckling stresses, which can be explained by the involved deformation mechanisms.

Table 2. Finite element discretization for different core configurations.

Core configuration	IHC	DAH1	DAH2
Number of FE	18,900	27,324	35,856

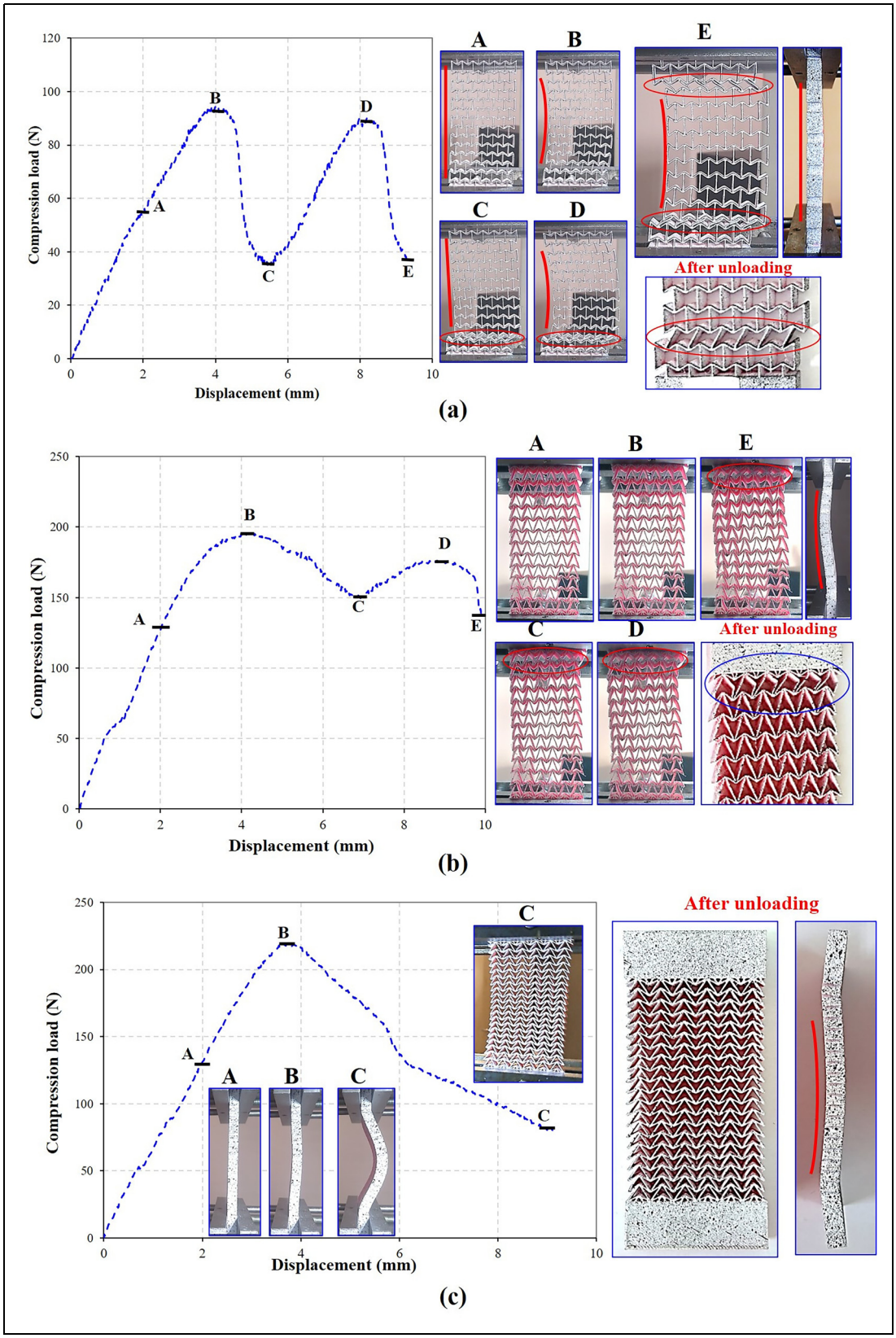

Figure 6. Load–displacement evolution and deformed shapes of cellular structures at characteristic points and after unloading: (a) C_IHC, (b) C_DAH1, and (c) C_DAH2.

Indeed, the IHC cellular structure exhibits in-plane overall buckling as well as unit cell buckling by collapse of cell walls with plastic yielding, while DAH2 undergoes global elastic buckling.

Buckling of sandwich panels with auxetic core

The compressive responses of sandwich panels with auxetic cores, consisting of IHC, DAH1 and DAH2 unit

cells, are illustrated in Figure 7(a), (b) and (c), respectively. The deformed shapes at different characteristic points on the load–displacement curves are embedded in the figures to track the specimen deformation mechanisms. All of the structures demonstrated linear elastic behavior up to the limit point B, which corresponds to the critical buckling stress. In the pre-buckling stage, the sandwich panel remains elastic and straight until the maximum stress is reached, indicating structure failure by out-of-plane deflection that leads to a load decrease. As shown in Figure 7(a), at the beginning of the post-buckling stage, the sandwich panel with IHC core exhibits global buckling. At a displacement of 6.5 mm (Point C), a transition from global buckling to local face wrinkling occurs, resulting in a sharp decrease in compressive stress. It is worth noting that the geometric instability of the IHC sandwich panel is coupled with plastic yielding of the facesheet, as observed on the structure after unloading. Figure 7(b) shows that the DAH1 sandwich panel buckles at approximately the same critical load as the IHC panel. The initial buckling mode is of global buckling type, followed by intercell plastic buckling. It can be noticed, from the deformed structure after unloading, that the facesheet undergoes plastic yielding. By increasing the density of the DAH core, the critical buckling stress increases, and the failure mode is solely global buckling, resulting in out-of-plane deflection as shown in Figure 7(c). The deformed shape after unloading shows that plastic buckling occurs throughout the structure. The difference in failure modes for these sandwich panels is mainly due to the unit-cell shape and the core density.

To gain further insight into the effect of these parameters on the buckling of sandwich panels, the nominal and specific critical buckling stresses are reported in Table 4. Nominal stresses have been calculated by dividing the measured load by the cross-sectional area of the two facesheets, as recommended by the standard test method ASTM C364.

According to the values provided in Table 4, the IHC and DAH1 sandwich panels show approximately the same critical buckling stress. However, the specific buckling stress is higher for the IHC sandwich panel. This indicates that, despite having similar nominal buckling loads, the IHC panel is more efficient in terms of load-carrying capacity relative to its density. On the other hand, the sandwich panels with the DAH2 core, which presents a higher density, exhibit the lowest specific buckling stress. This suggests that, although DAH2 panels can bear higher loads due to their density, their efficiency in terms of stress relative to their density is lower. Notably, the DAH2 panels do not exhibit local buckling in the facesheet, which can be attributed to the lower cell size and higher density that distribute the load more evenly and prevent localized failure.

Numerical results

Validation of the finite element model

To validate the developed FEM, the load evolution against the axial displacement, as well as the successive deformed shapes, have been compared to their experimental counterparts. To avoid redundancy, only the numerical results of the IHC cellular structure are depicted in Figure 8. As we are mainly interested in evaluating the buckling behavior, the simulation has been limited to the post-buckling stage up to the first densification point (Point C). Beyond this point, general contact would have needed to be introduced to control the cell wall interactions, but this would have significantly increased the computational cost. The numerical results align well with the experimental data, with discrepancy in the critical buckling load remaining below 9%. In fact, it is noteworthy that good agreement has been observed for the three simulated structures. In addition to accurately predicting the load evolution, the developed model is capable of handling the deformation process, tracking the buckling failure mode, and post-buckling response based on the Riks technique. As can be seen from the insets in Figure 8, the numerical simulation shows in-plane buckling of the auxetic structure at limit point B, followed by local buckling of cell walls and densification at point C, similar to the experimental results. In the pre-buckling stage, the lateral shrinkage characterizing the auxetic effect is easily visualized through the finite element results.

Figure 9 depicts the superimposed deformed and undeformed shapes, with lateral displacement distribution (along the y-direction) of the IHC, DAH1 and DAH2 structures at an imposed displacement (along the x-direction) of approximatively 2 mm. As shown in this figure, the IHC and DAH1 structures display lateral shrinkage, indicated by blue arrows, with symmetric behavior measuring ± 0.52 mm and ± 0.99 mm, respectively. However, the DAH2 structure exhibits an out-of-plane deflection, leading to asymmetric in-plane shrinkage values of $+0.73$ mm and -0.4 mm. It can also be noted that the most auxetic structure, DAH1, shows the highest

Table 3. Specific critical buckling stress and failure modes of C-specimens.

Auxetic cell	Critical buckling stress (MPa)	Density (g/mm^3)	Specific critical buckling stress (MPa/g/mm^3)	Failure mode
IHC	0.292	0.000192	1522.63	In plane buckling + plastic yielding
DAH1	0.572	0.000228	2508.10	In plane buckling + plastic yielding
DAH2	0.645	0.000288	2240.14	Global elastic buckling

lateral displacement. The higher lateral displacement may explain the resistance of the DAH1 structure to compressive loading, resulting in a higher critical buckling load.

To check the ability of the developed model to predict the buckling behavior of the sandwich panels, the load evolution against compressive displacement for the IHC core has been plotted in Figure 10. Similar to the

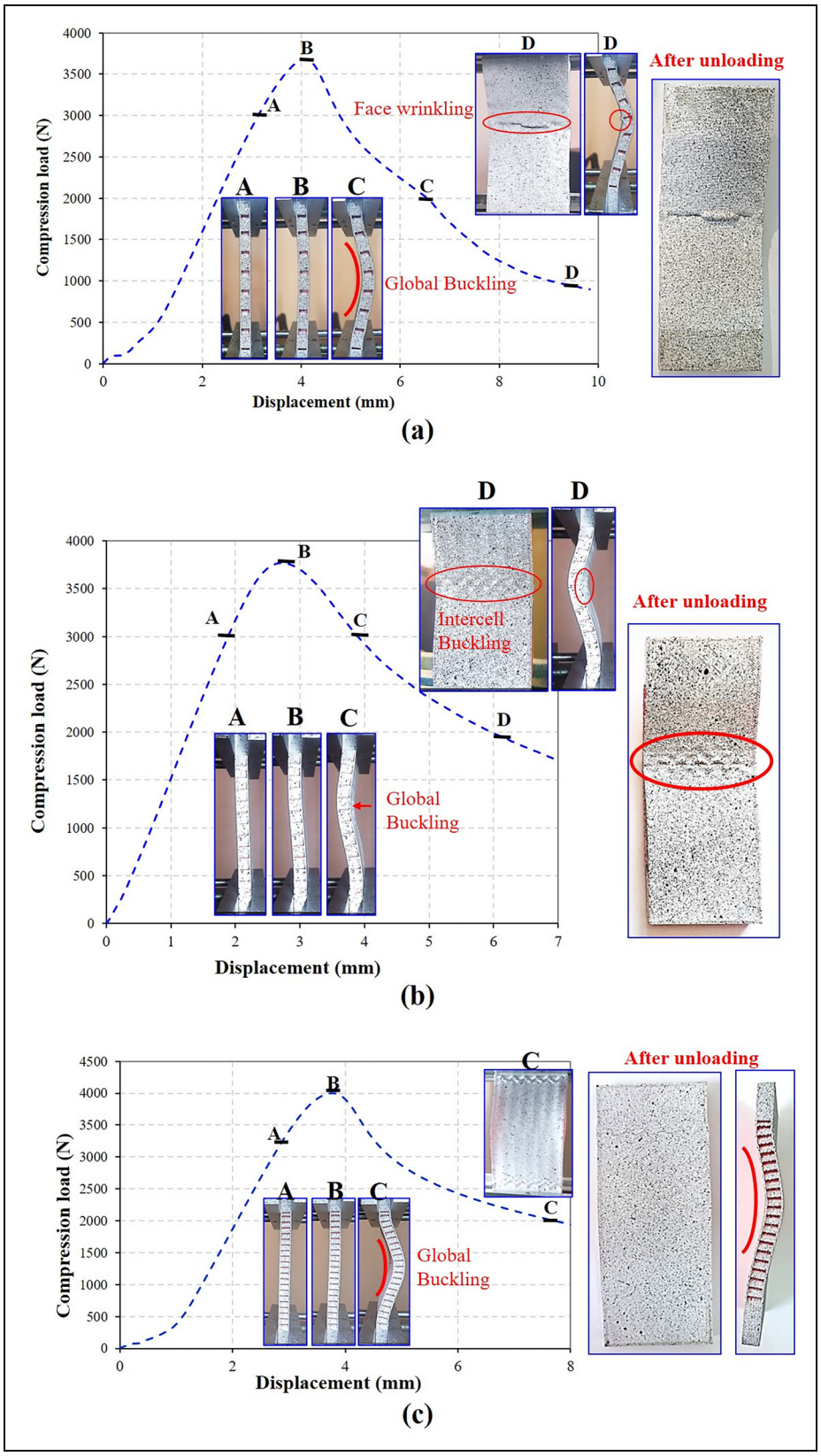

Figure 7. Load–displacement evolution and deformed shapes of sandwich panels at characteristic points and after unloading: (a) SP_IHC, (b) SP_DAH1, and (c) SP_DAH2.

Table 4. Specific critical buckling stress and failure modes of SP-specimens.

Auxetic cell	Critical buckling stress (KPa)	Density (g/mm^3)	Specific critical buckling stress (MPa/g/mm^3)	Failure mode
IHC	46.59	0.000192	2.43 $^{e+}$5	Global buckling + face wrinkling + plastic yielding
DAH1	47.10	0.000228	2.07^{e+} 5	Global buckling + intercell buckling + plastic yielding
DAH2	50.00	0.000288	1.74^{e+} 5	Global buckling + plastic yielding

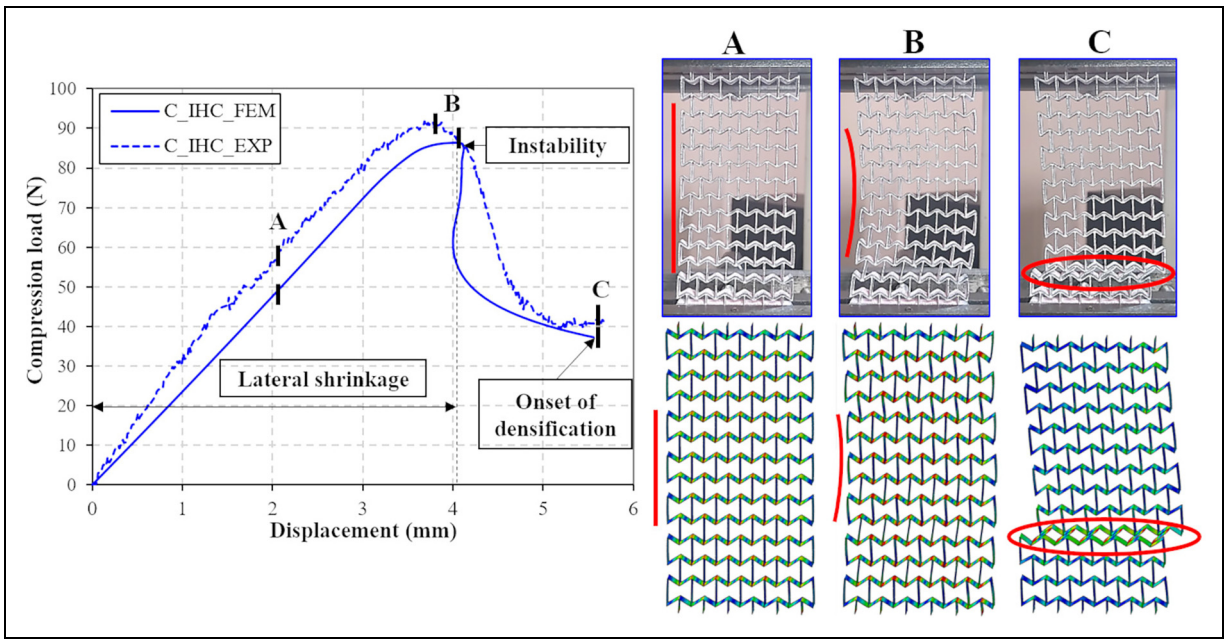

Figure 8. Comparison of numerical and experimental results: load–displacement evolution and deformed shapes of C_IHC specimen.

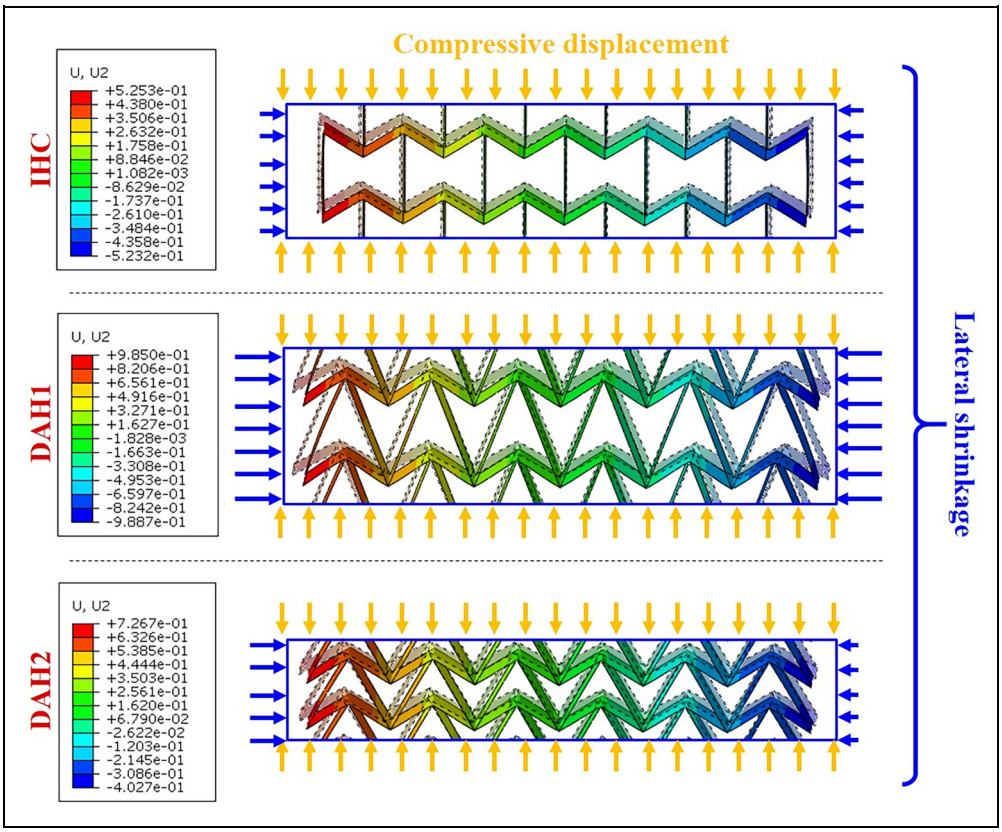

Figure 9. Lateral shrinkage of C_IHC, C_DAH1, and C_DAH2.

experimental results, the load increases linearly until the limit strength (limit point B) of the structure is reached. Comparing the numerical and the experimental critical buckling loads, the relative deviation is lower than 7%, thus demonstrating the good accuracy of the developed model. However, the numerical model exhibits stiffer behavior than the experimental counterpart, which can be attributed to the rigidity of the experimental device.[31]

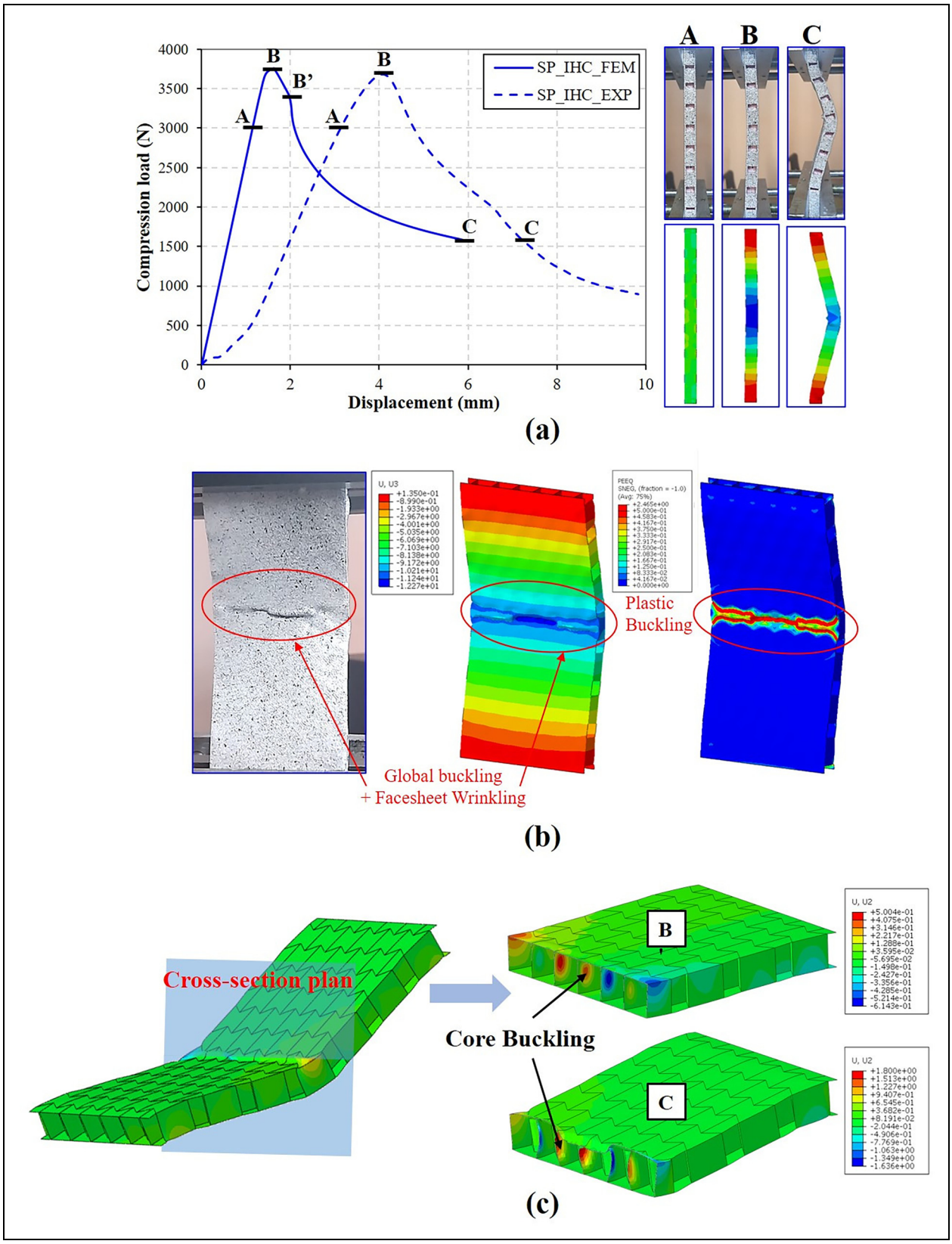

Figure 10. Comparison of numerical and experimental results of SP_IHC specimen: (a) load–displacement evolution, (b) failure mode, (c) core buckling.

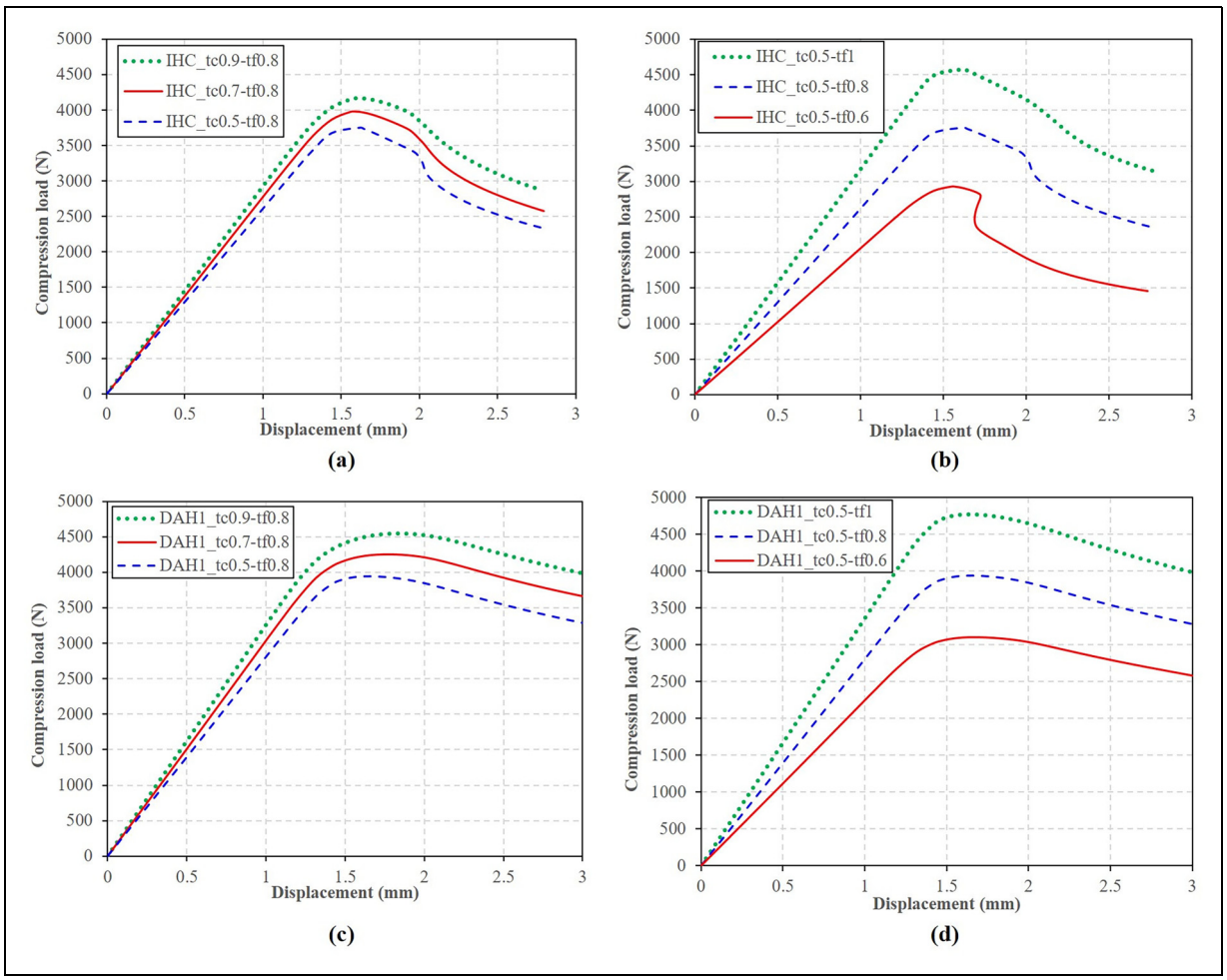

Figure 11. Load–displacement evolution: (a) IHC with various cell-wall thicknesses, (b) IHC with various facesheet thicknesses, (c) DAH1 with various cell-wall thicknesses, (d) DAH1 with various facesheet thicknesses.

It is important to note that this difference in the curve slope has not been detected in the cellular auxetic structure, as the specimen is very soft. In addition, the evolution of the specimen deformation from the pre-buckling to the post-buckling stages shows almost the same deformation mechanisms as the experimental results. Figure 10(b) depicts the failed sandwich panel at the post-buckling stage (Point C) using the displacement and equivalent plastic deformation (PEEQ) distributions. The numerical simulations establish the same failure modes as those observed experimentally. It is clear that the IHC sandwich panel undergoes global buckling and plastic wrinkling of the facesheet. An advantage of using the FE simulations is their ability to reveal the deformation mode of the core. As shown in Figure 10(c), at the post-buckling stage (Points B' and C), the IHC cell walls buckle underneath the facesheet wrinkles, which can explain the facesheet failure. It is relevant to note that the onset of the cell-wall buckling at point B' is associated with a sharper decrease in the compression load. This finding demonstrates the significant effect of core thickness and height on the buckling behavior of sandwich panels, as addressed in the literature.[32]

Effect of cell-wall and facesheet thickness

Considering the aforementioned results, it is clear that the Poisson ratio of the auxetic structure has a significant effect on the buckling behavior and deformation mechanism of the cellular structures, which is in good agreement with the literature.[7] However, this effect is attenuated in the sandwich panel, as the structure is stiffened by compressive skins (facesheets). To highlight the influence of the core and the facesheets on the global response of the sandwich panel, numerical simulations of sandwich panels with varying cell-wall thicknesses and facesheet thicknesses have been conducted for both the IHC and DAH1 cells. To assess the impact of cell-wall thickness t_c, the facesheet thickness t_f has been kept constant at 0.8 mm, while the cell-wall thickness t_c has been varied at 0.5, 0.7, and 0.9 mm, as illustrated in Figure 11(a) and (c). Conversely, to investigate the effect of facesheet thickness t_f, the cell-wall thickness t_c has been fixed at 0.5 mm, while the facesheet thickness t_f has been adjusted to 0.6, 0.8, and 1 mm, as shown in Figure 11(b) and (d).

It can be seen from Figure 11 that both the cell-wall and facesheet thicknesses strongly influence the critical

buckling load of the sandwich panel. Notably, the panel skin thickness has a more significant effect for both of auxetic cell types. For instance, in the IHC sandwich panel, an increase in the facesheet thickness of 25%, which corresponds to a panel mass rise of approximately 14%, results in a 21% increase in the critical buckling load. By contrast, increasing the cell-wall thickness by 40%, which results in a panel mass increase of about 17%, leads to improvement in the load-carrying capacity of only 6%. Similar observations can be made for the DAH1 sandwich panel, thus demonstrating the greater influence of the facesheet thickness, as compared to the core, on the panel response. This may explain the closely aligned critical buckling loads observed in both the IHC and DAH1 panels. Furthermore, the facesheet thickness exhibits a notable effect on the post-buckling behavior, especially in the IHC sandwich panel. In this case, thin facesheets lead to snap-back behavior. This can be attributed to the facesheet thickness and the internal cell size. Indeed, although the IHC and DAH1 cells have approximately the same width and length, the internal cell size in the IHC shape is larger, which affects the overall structural stability.

Conclusions

In the present study, the buckling behavior and failure modes of auxetic structures and sandwich panels with auxetic cores have been comprehensively investigated based on experimental tests and FE simulations. The numerical results showed good agreement with the experimental data, thus validating the developed model and demonstrating the Riks method ability to predict the plastic buckling and failure mechanisms of metamaterials and sandwich panels with auxetic cores. The responses of auxetic structures designed with the inverted honeycomb (IHC) and the double arrowhead (DAH) cells with different densities have been compared. The results indicate that the auxetic nature and density enhance the buckling resistance of cellular structures under compressive loading, allowing a higher critical buckling stress in the DAH configuration. Additionally, these parameters significantly affect the failure modes of the sandwich panels, particularly the local buckling of the facesheets, which is crucial for the bending resistance of a sandwich panel. The auxetic sandwich panel with an IHC core exhibits plastic buckling and facesheet wrinkling due to cell-wall buckling and a large internal cell surface. In this case, the facesheet failure becomes more pronounced, leading to snap-back behavior when the facesheet thickness is reduced. Increasing the core auxeticity results in a dominant global buckling mode, despite a reduced influence on load-carrying capacity. Additionally, increasing core density by adjusting cell dimensions made the sandwich panel more susceptible to global buckling, while reducing the likelihood of core failure. In future work, the developed model will be further investigated to explore the effects of geometric and material parameters on the plastic buckling and failure modes of sandwich panels with auxetic cores.

Declaration of conflicting interests

The authors declared no potential conflicts of interest with respect to the research, authorship, and/or publication of this article.

Funding

The authors received no financial support for the research, authorship, and/or publication of this article.

ORCID iDs

M BelHadjAmor https://orcid.org/0000-0003-1890-617X
S Mezlini https://orcid.org/0000-0003-1209-4246

References

1. Liu X, Zhong Y, Liu R, et al. Buckling and post-buckling analysis of butterfly-shaped auxetic core sandwich plates based on variational asymptotic method. *Thin-Walled Struct* 2023; 184: 110464.
2. Evans KE, Nkansah MA, Hutchinson IJ, et al. Molecular network design. *Nature* 1991; 353: 124.
3. Montgomery-Liljeroth E, Schievano S and Burriesci G. Elastic properties of 2D auxetic honeycomb structures- a review. *Appl Mater Today* 30. Epub ahead of print 1 February 2023. DOI: 10.1016/j.apmt.2022.101722.
4. Alderson KL, Fitzgerald A and Evans KE. The strain dependent indentation resilience of auxetic microporous polyethylene. *J Mater Sci* 2000; 35: 4039–4047.
5. Jin S, Korkolis YP and Li Y. Shear resistance of an auxetic chiral mechanical metamaterial. *Int J Solids Struct* 2019; 174–175: 28–37.
6. Khoa ND, Bohara RP, Ghazlan A, et al. Novel hierarchical bioinspired cellular structures with enhanced energy absorption under uniaxial compression. *Aerosp Sci Technol* 147. Epub ahead of print 1 April 2024. DOI: 10.1016/j.ast.2024.108995.
7. Dong Z, Li Y, Zhao T, et al. Experimental and numerical studies on the compressive mechanical properties of the metallic auxetic reentrant honeycomb. *Mater Des* 182. Epub ahead of print 15 November 2019. DOI: 10.1016/j.matdes.2019.108036.
8. Zhang XY, Ren X, Zhang Y, et al. A novel auxetic metamaterial with enhanced mechanical properties and tunable auxeticity. *Thin-Walled Struct* 174. Epub ahead of print 1 May 2022. DOI: 10.1016/j.tws.2022.109162.
9. Fu MH, Chen Y and Hu LL. A novel auxetic honeycomb with enhanced in-plane stiffness and buckling strength. *Compos Struct* 2017; 160: 574–585.
10. Larsen UD, Signund O and Bouwsta S. Design and fabrication of compliant micromechanisms and structures with negative poisson's ratio. *J Microelectromechanical Syst* 1997; 6: 99–106.
11. Bohara RP, Linforth S, Nguyen T, et al. Novel lightweight high-energy absorbing auxetic structures guided by topology optimisation. *Int J Mech Sci* 211. Epub ahead of print 1 December 2021. DOI: 10.1016/j.ijmecsci.2021.106793.
12. Khoshgoftar MJ, Barkhordari A, Limuti M, et al. Bending analysis of sandwich panel composite with a re-entrant lattice core using zig-zag theory. *Sci Rep* 12. Epub ahead

of print 1 December 2022. DOI: 10.1038/s41598-022-19930-x.
13. Xiao P, Yifeng Z, Jie S, et al. Global buckling analysis of composite honeycomb sandwich plate with negative Poisson's ratio (CHSP-NPR) using variational asymptotic equivalent model. *Compos Struct* 264. Epub ahead of print 15 May 2021. DOI: 10.1016/j.compstruct.2021.113721.
14. Xiao P, Bin L, Vescovini R, et al. Optimal design of composite sandwich panel with auxetic reentrant honeycomb using asymptotic equivalent model and PSO algorithm. *Compos Struct* 328. Epub ahead of print 15 January 2024. DOI: 10.1016/j.compstruct.2023.117761.
15. Zhen W, Xinlong Y, Wengen L, et al. A VAM-based equivalent model for triangular honeycomb sandwich panels: comparison with numerical and experimental data. *Materials (Basel)* 2022; 15: 4766.
16. Kaman MO, Solmaz MY and Turan K. Experimental and numerical analysis of critical buckling load of honeycomb sandwich panels. *J Compos Mater* 2010; 44: 2819–2831.
17. Zhang XM, Wang YC and Su MN. Experimental, numerical and analytical study to develop a design method for bending and shear resistances of 3D printed beetle elytron inspired sandwich plate (beetle elytron plate). *Thin-Walled Struct* 183. Epub ahead of print 1 February 2023. DOI: 10.1016/j.tws.2022.110371.
18. Li X, Yang H, Zhang H, et al. Failure mechanisms of fluted-core sandwich composite panels under uniaxial compression. *Compos Struct* 303. Epub ahead of print 1 January 2023. DOI: 10.1016/j.compstruct.2022.116317.
19. Vinson JR. Optimum design of composite honeycomb sandwich panels subjected to uniaxial compression. *AIAA J* 1986; 24: 1690–1696.
20. Sun G, Huo X, Chen D, et al. Experimental and numerical study on honeycomb sandwich panels under bending and in-panel compression. *Mater Des* 2017; 133: 154–168.
21. Zhang XM, Wang YC, Foster ASJ, et al. Elastic local buckling behaviour of beetle elytron plate. *Thin-Walled Struct* 165. Epub ahead of print 1 August 2021. DOI: 10.1016/j.tws.2021.107922.
22. Zhang XM, Wang YC, Su MN, et al. Elastic–plastic buckling behaviour of beetle elytron plate with simple, fixed and flexible core supports. *Thin-Walled Struct* 179. Epub ahead of print 1 October 2022. DOI: 10.1016/j.tws.2022.109534.
23. BelhadjAmor M, Ben Bettaieb M, Mezlini S, et al. Development and implementation of a new computational strategy for the prediction of elastoplastic buckling International Journal of Applied Mechanics. *Int J Appl Mech*. DOI: https://doi.org/10.1142/S1758825124500911.
24. Riks E. An incremental approach to the solution of snapping and buckling problems. *Int J Solids Struct* 1979; 15: 529–551.
25. Killpack M and Abed-Meraim F. Limit-point buckling analyses using solid, shell and solid-shell elements. *J Mech Sci Technol* 2011; 25: 1105–1117.
26. Lakes R. Foam structures with a negative poisson's ratio. *Science (80-)* 1987; 235: 1038–1040.
27. Ingrole A, Hao A and Liang R. Design and modeling of auxetic and hybrid honeycomb structures for in-plane property enhancement. *Mater Des* 2017; 117: 72–83.
28. Qiao JX and Chen CQ. Impact resistance of uniform and functionally graded auxetic double arrowhead honeycombs. *Int J Impact Eng* 2015; 83: 47–58.
29. Raise3D Premium PLA Technical Data Sheet. *Raise 3D*, https://s1.raise3d.com/2023/02/Raise3D-Premium_PLA_TDS_V5.1_EN.pdf?_gl=1*4t0i3t*_gcl_au*MTc5NTkyMTI4MS4xNzI5NTA1NTk5 (last accessed 21 October 2024).
30. Hutchinson JW and Budiansky B. Analytical and numerical study of the effects of initial imperfections on the inelastic buckling of a cruciform column. In: B Budiansky (ed) *Buckling of structures*. Berlin, Heidelberg: Springer, 1976; pp.98–105.
31. Miller W, Smith CW and Evans KE. Honeycomb cores with enhanced buckling strength. *Compos Struct* 2011; 93: 1072–1077.
32. Scarpa F, Blain S, Lew T, et al. Elastic buckling of hexagonal chiral cell honeycombs. *Compos Part A Appl Sci Manuf* 2007; 38: 280–289.